MANDEL & CRYER PROBLEMS FOR FLUID-SATURATED FOAMS WITH NEGATIVE POISSON'S RATIO

Michio Kurashige, Keiichi Sato and Kazuwo Imai Iwate University, Department of Mechanical Engineering, Morioka, Iwate 020-8551, Japan

Summary The advent of various foams with negative Poisson's ratio has interested us in how these foams will behave when they are saturated with fluid. To explore this behavior, we have solved 2D and 3D versions of the Mandel and Cryer problems in a unified manner. The results show that much more remarkable Mandel-Cryer effect and additional interactions between the elastic deformation and pore fluid diffusion are observed for the negative Poisson's ratio than for the conventional one.

INTRODUCTION

It has been well known that the value of Poisson's ratio thermodynamically ranges from -1.0 to 0.5 for isotropic linear elastic materials, although the negative ratios are counterintuitive and real conventional isotropic materials have the positive ratios. In 1987, Lakes [1] created polymer and metal foams having negative Poisson's ratios and, following this creation, he and his coworkers have explored various characteristics of such materials and discussed their microstructures and their real and possible applications.

This advent of foamed polymers and metals with negative Poisson's ratios have stirred our interest and imagination in how these unconventional foams will behave and what phenomena their negativeness will bring when they are fully saturated with fluid. To explore these behavior and phenomena, we picked up the four problems: the original Mandel problem [2] and a corresponding axisymmetric problem, and the original Cryer problem and a corresponding plane strain problem. We call these four problem "2D and 3D, Mandel and Cryer problems." We selected these four problems among many other problems because we expected that they manifest most remarkable interactions between the elastic deformation of sample skeletons and pore fluid flow. We analytically solved these problems in the Laplace transform space in a unified manner and numerically inverted the solutions into the real time space.

FOUR PROBLEMS TO SOLVE

To describe the problems, we introduce the Cartesian, cylindrical polar and spherical polar coordinate systems: (x,z) (r,θ,z) and (r,φ,θ) . The four problems are presented in Fig.1 together with their boundary conditions, where only the statically equivalent, lower halves of a circular cylinder and a sphere in the Cryer problems are shown to make it more convenient to discuss the results of solutions. For all problems, the initial conditions are that all variables are zero at time t = 0 and the loading is a step-like one; in addition, the basic equations applicable for an irrotational displacement field are used. In the figure, $\sigma_0 = P_0/(\pi a^2)$, which means the average axial compressive stress for the Mandel problem and pressure loading on the surface for the Cryer problem.

SOLUTIONS IN LAPLACE TRANSFORM SPACE

Only the solutions for the 2D Cryer problem are presented here, for the economy of space and because they have not seen in literature.

$$\overline{p}(r,s) = \left(\frac{\sigma_0}{s}\right) \frac{v_u - v}{\eta} \left\{ 1 - \frac{I_0(\sqrt{s/cr})}{I_0(\sqrt{s/ca})} \right\} / F(s), \tag{1}$$

$$\overline{p}(r,s) = \left(\frac{\sigma_0}{s}\right) \frac{v_u - v}{\eta} \left\{ 1 - \frac{I_0(\sqrt{s/cr})}{I_0(\sqrt{s/ca})} \right\} / F(s), \tag{1}$$

$$\overline{\sigma}_r(r,s) = \left(-\frac{\sigma_0}{s} \right) \left[1 + 2(v_u - v) \left\{ \frac{I_1(\sqrt{s/ca})}{(\sqrt{s/ca})I_0(\sqrt{s/ca})} - \frac{I_1(\sqrt{s/cr})}{(\sqrt{s/cr})I_0(\sqrt{s/ca})} \right\} / F(s) \right\}, \tag{2}$$

$$\overline{\sigma}_{\theta}(r,s) = \left(-\frac{\sigma_0}{s} \right) \left[1 + 2(v_u - v) \left\{ \frac{I_1(\sqrt{s/ca})}{(\sqrt{s/ca})I_0(\sqrt{s/ca})} + \frac{I_1(\sqrt{s/cr})}{(\sqrt{s/cr})I_0(\sqrt{s/ca})} - \frac{I_0(\sqrt{s/cr})}{I_0(\sqrt{s/ca})} \right\} / F(s) \right\}, \tag{3}$$

$$\overline{\sigma}_{\theta}(r,s) = \left(-\frac{\sigma_0}{s}\right) \left[1 + 2(v_u - v)\left\{\frac{I_1(\sqrt{s/ca})}{(\sqrt{s/ca})I_0(\sqrt{s/ca})} + \frac{I_1(\sqrt{s/cr})}{(\sqrt{s/cr})I_0(\sqrt{s/ca})} - \frac{I_0(\sqrt{s/cr})}{I_0(\sqrt{s/ca})}\right\}/F(s)\right],\tag{3}$$

with

$$F(s) = (1-v) - 2(v_u - v) \frac{I_1(\sqrt{s/ca})}{(\sqrt{s/ca})I_0(\sqrt{s/ca})}, \quad \eta = \frac{\alpha(1-2v)}{2(1-v)}, \quad \alpha = \frac{3(v_u - v)}{B(1-2v)(1+v_u)}, \tag{4}$$

where v and v_u are Poisson's ratios in the drained and undrained states; B denotes Skempton's coefficient and c the coefficient of pore fluid diffusion. The bar over variables means the Laplace transform with its parameter s. With all other notations, see Fig.1.

RESULTS AND DISCUSSIONS

Numerical calculations have been carried out only for the incompressible constituents model ($v_u = 0.5, B = 1.0$), because the bulk modulus of drained foams is much smaller than that of pore fluid (e.g., water) and skeleton material (e.g., polyester and cupper). In all figures, $\rho = r/a$ and $\tau = t/(a^2/c)$ are the nondimensional radial coordinate and time.

The Mandel-Cryer effect for the four problems is shown in the case of v = -0.8 in Fig.2. We can see from it that the effect is very remarkable for this negative Poisson's ratio and that the peak pressure is higher for the Cryer problems than for the Mandel ones and for the 3D problems than for the 2D ones. The analysis shows that the Mandel-Cryer effect is more remarkable for decreasing Poisson's ratio. It is also shown that the peak pressures in the limit v = -1 for the Cryer and Mandel problems are 2.5 and 2.0 times those immediately after loading, respectively. In what follows, we will focus on the 3D Mandel problem, because it corresponds to usual compression tests of a circular cylinder. Fig.3 shows variation with time of circumferential stress component $-\sigma_{ heta}$ for various radius positions. At very deep positions, that stress starts from zero, goes up to the peak, and then decreases and vanishes, as corresponds to the variation of pore fluid pressure. In contrast, at the shallow positions it has the minimum value at some time after loading. It must be noted that its initial value is zero for $\rho < 1$ while $-\sigma_{\theta}/\sigma_{0} = (v_{u}-v)/(1-v)(1+v_{u})$ at $\rho = 1$, which is not zero; there exists a discontinuity at the cylinder surface. The same things appear in axial stress $-\sigma_z$. Similar behavior is also seen for the Cryer problem, as may be understood from the halved disc and sphere in Fig.1.

Figure 4 depicts time variation of radial displacement u_r at the cylinder surface for various Poisson's ratios. It is found that the cylinder of negative Poisson's ratio under abrupt

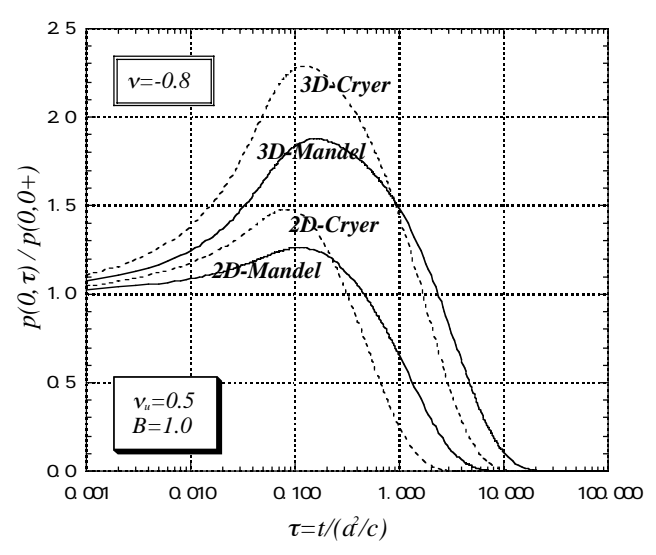


Figure 2 Mandel-Cryer effect for four problems

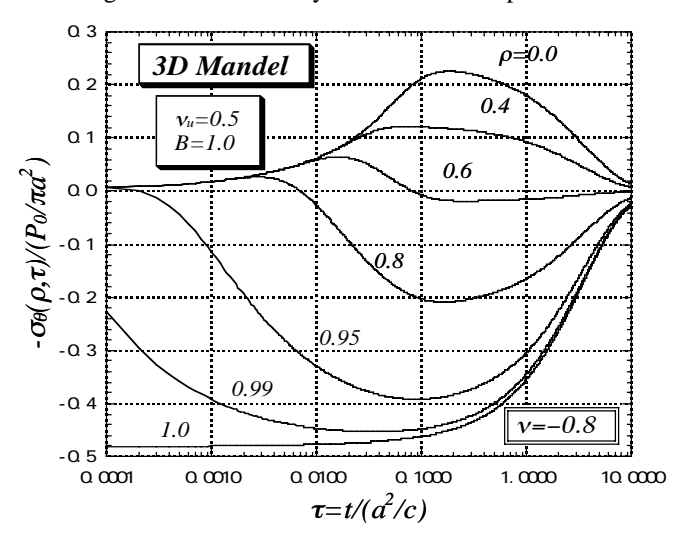
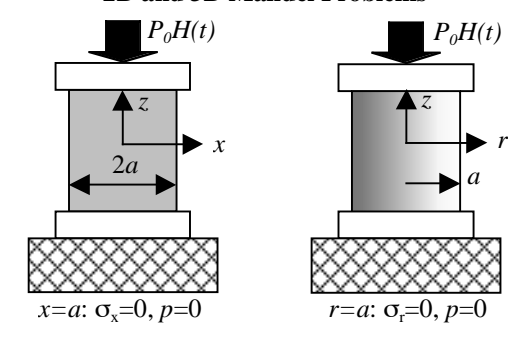


Figure 3 Hoop stress for various positions

2D and 3D Mandel Problems



2D and 3D Cryer Problems

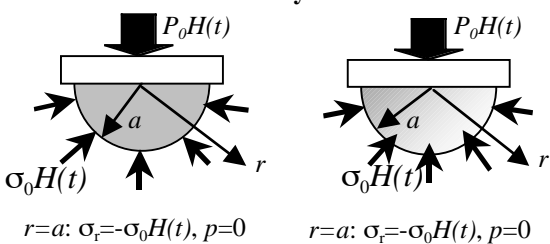


Figure 1 Four problems to solve

compression expands just after loading, gradually shrinks, and finally becomes slenderer than the original one, as is interesting and intuitively well understandable. It should be added that this displacement is normalized by using Young's modulus, which are reported to decrease with decreasing Poisson's ratio but its decrease is not so big.

CONCLUSIONS

We have demonstrated various interesting behaviors of fluid-filled poroelastic samples with negative Poisson's ratio.

References

- [1] Lakes, R., Science, 237, 1038-1040 (1987).
- [2] Mandel, J., Geotechnique, 3, 287-299 (1953).

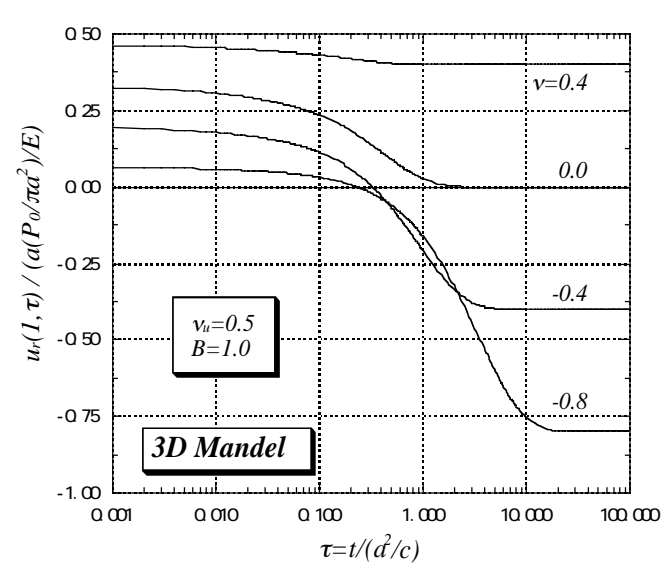


Figure 4 Radial displacement at the cylinder surface